RSC Advances

ROYAL SOCIETY OF CHEMISTRY

www.rsc.org/advances

RCS Advances

ARTICLE

Towards computational design of zeolite catalysts for CO_2 reduction

Received 00th January 20xx,
Accepted 00th January 20xx

DOI: 10.1039/x0xx00000x

www.rsc.org/

A. W. Thornton,[a,†] D. A. Winkler,[a,b] M. S. Liu,[c] M. Haranczyk[d] and D. F. Kennedy[a]

Carbon dioxide, an energy waste by-product with significant environmental consequences can be utilized and converted into useful chemical products such as formic acid, formaldehyde, methanol or methane, but more energy and cost efficient catalytic processes are required. Here we develop the methodology for the intelligent selection of porous zeolites for dual-adsorption of hydrogen and carbon dioxide as templates for preparing the optimal catalytic environment for carbon dioxide reduction. Useful zeolite catalysts were computationally screened from over 300 thousand zeolite structures using a combination of molecular simulation and machine-learning techniques. Several of the top candidates were very promising energy-efficient templates for catalysis with the potential to perform at 50 % above conventional reactors. It is also found that an optimal cavity size of around 6 Å is required to maximize the change in entropy-enthalpy upon adsorption with a maximum void space > 30 % to boost product formation per volume of material.

Introduction

The environmental impact of global CO_2 levels is well documented.[3, 4] For the past decade the focus of atmospheric remediation has been on long term storage of CO_2 via geosequestration to mitigate the effect of societies use of fossil fuels. Increasingly, there is a move away from the energy intensive process of carbon capture and storage (CCS) to carbon capture and utilization (CCU).[3] Approaches to CCU may be as simple as new large scale uses for supercritical CO_2, or application of CO_2 as growth medium for algal growth. An increasingly attractive alternative utilization method is the catalyzed chemical transformation of CO_2 into useful and saleable chemical feedstocks and fuels such as formic acid, formaldehyde, methanol and methane.[2, 5-8] Hydrogen is a promising fuel but it lacks the energy density for practical use. Conversion of CO_2 and hydrogen into liquid fuels such as methane or methanol is more desirable from a convenience and energy density perspective. However, significant improvement in catalyst technology for CO_2 conversion is required for CCU to become an economically viable alternative. Recent advances in catalytic include the direct synthesis of formic acid from carbon dioxide by hydrogenation using a ruthenium catalyst by Moret *et al.*[9] and the photothermal reduction of CO_2 to methane in the gas phase over nanocatalysts by Meng *et al.*[10] Moreover, Graciani *et al.*[11] recently reported methanol synthesis from CO_2 with novel composites. While these studies demonstrate advances in CO_2 conversion, the discovery procedure is limited to a small set of materials through experimental trial and error.

Virtual screening is a method that broadly combines computational algorithms for selecting promising candidates from a large library of materials.[12] In many fields of materials science, there are an unlimited number of possible structures to choose from for a particular application. Combinatorial methods, in combination with high-throughput synthesis and characterization methods, have attempted to address this challenge by increasing the number of candidates that can be tested, but this requires large amounts of time and resources.[13] Increasing recognition of the enormity of materials compositional and property space is also driving alternative methods for materials discovery, such as computational design, virtual screening, and materials evolutionary methods. Virtual screening or high-throughput computational screening provides an inexpensive and rapid method to pre-screen candidates before pursuing synthesis. Successful examples of virtual screening include:

- the selection of porous adsorbents for the separation of linear, mono-branched, and di-branched isomers of alkanes for petrochemical applications.[14]
- the selection of zeolitic imidazolate framework (ZIF)-based membranes for clean energy applications including

[a] CSIRO Manufacturing Flagship, Private Bag 10, Clayton South MDC, Victoria 3169, Australia.
[b] Monash Institute of Pharmaceutical Sciences, 390 Royal Parade, Parkville 3052, Australia.
[c] CSIRO Digital Productivity and Services Flagship, Private Bag 10, Clayton South MDC, Victoria 3169, Australia.
[d] Lawrence Berkeley National Laboratory, Computational Research Division, Berkeley, CA 94720 USA
†Corresponding author: Aaron W. Thornton, Aaron.Thornton@csiro.au
Electronic Supplementary Information (ESI) available: Inverse-IAST formulation, force field tables and complete list of top candidates. See DOI: 10.1039/x0xx00000x

land fill gas purification, post-combustion CO_2 separation and pre-combustion H_2 separation.[15]
- the selection of zeolites and ZIFs for carbon dioxide capture.[16]
- the selection of metal-organic frameworks (MOFs) for carbon dioxide separation.[17]
- the selection of MOF analogues for water adsorption.[18]
- the selection of compounds for molecular docking in proteins for pharmaceutical inhibitors.[19]
- the selection of MOFs for methane storage.[20]

We have modified the methology of virtual screening and applied it to predict the dual-adsorption of gases for catalyzed reactions in this study, depicted in Figure 1. Porous catalysts such as zeolites offer large surface areas and active sites available for CO_2 conversion and they can be 'tuned' to optimize their performance. There are ca. 200 known ideal silica zeolites[21] and over a billion hypothetical zeolites[22] developed from the bonding principles between silicon and oxygen. With an abundant database of structures there is an opportunity and a computational challenge to select the promising candidates that could act as excellent templates for porous catalysts. An important step in heterogeneous catalysis is the adsorption step before catalysis. The methodology for predicting gas adsorption within nanoporous materials is well established.[18, 23-25] Therefore we predict the gas stoichiometric adsorption properties within zeolite candidates and use this information to select the most promising zeolite for catalysis.

Finally, machine learning methods based on Quantitative Structure-Property Relationships (QSPR) models offer a useful framework for interpreting the screening results and targeting the most important structural characteristics for further discovery.[26, 27] QSPR models were utilized by Fernandez *et al.*[27] to investigate MOFs for methane storage, which revealed an optimal range of, pore sizes and void fraction. With a growing dataset of structures, QSPR models are needed to explore regions of the materials landscape unreachable by more computationally-intensive methods such as molecular dynamics and quantum chemistry. Other examples of QSPR modelling include the prediction of C_{60} solubility in various solvents, thermal conductivity of nanomaterials, operating conditions for optimal catalysis and bio-compatibility of polymeric materials.[26, 28-32] Here the QSPR method is applied to a relatively simple system to predict the gas adsorption and thermodynamic properties of zeolites based on a few structural descriptors.

Methodology

Virtual screening studies require a number of key components, such as the atomic structures, the structural descriptors (void fraction, surface area, heat of adsorption etc.), and the materials properties predicted from simulation. Here we describe the zeolite structures, the method for calculating descriptors, and the method for simulating material properties.

Zeolite Database

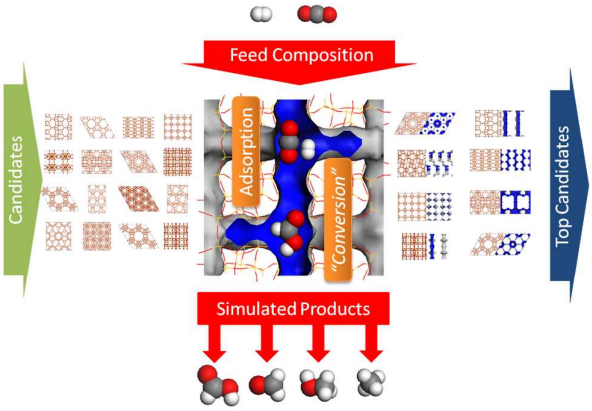

Fig. 1 Virtual screening workflow for predicting stoichiometric adsorption properties in preparation for catalysis.

There are approximately 200 experimental zeolite frameworks[33] and over a billion hypothetical zeolite structures constructed from the simple oxygen-silicon-oxygen bond repeated over all 230 space groups.[22, 34] Although many of the hypothetical structures are energetically inaccessible, there remains an enormous number of structures with a diverse range of pore morphology worthy of exploring. Previous screening work has narrowed the dataset down to around 300,000-500,000 energetically accessible structures, depending on the force field[16] used. Computational resource demands mean that it is impractical to simulate adsorption isotherms for the entire dataset; therefore a subset must be chosen to adequately represent the entire dataset. Martin *et al*. developed a similarity descriptor for zeolite structures that captures the shape and geometrical characteristics of pores.[35] Based on this, we selected a subset of 164 structures with maximal dissimilarity, i.e. with the most diverse set of pore characteristics. Overall, we analyze 167 ideal silica zeolites (after removing incomplete and energetically unfavourable frameworks), 164 hypothetical silica zeolites plus an additional 'smart' set of 60 zeolites chosen from the QSPR model described below.

Material Properties

Overall we are interested in the catalytic properties of each candidate material. Catalysis is a difficult phenomenon to predict because of the multiple steps and levels of theory involved. To reduce the problem, we begin with the adsorption step of feed gas mixture. There are four main steps in the catalytic process:

1. the diffusion of the reactant gases to the active sites within the material from the feed stock,
2. the adsorption of the reactant gases at the active sites,
3. the catalytic conversion of the reactant gases into products, and,
4. the desorption and diffusion of the products out of the material.

Each step contributes a thermodynamic and kinetic component to the overall efficiency. Here we focus on the

thermodynamics of the second step whereby the reactants, H_2 and CO_2, co-adsorb within the pores of the catalyst in preparation for the third step of catalytic conversion. The dual-adsorption ratios, or the stoichiometric adsorption properties of the material, play a critical role in the conversion efficiency. Upon adsorption there is a change in entropy and enthalpy that promotes the succeeding conversion steps. A large change in entropy and enthalpy upon adsorption will cause the reactants to bind into position and their internal bonds to become strained in preparation for reaction. In addition, the difference in adsorption between CO_2 and H_2 will determine the likely product to form due to stoichiometric considerations. Feed compositions can be tuned to optimize the adsorbed composition for the target product. Finally, the amount of pore volume and surface area will also govern the amount of product formation per volume of material. Therefore, optimization of CO_2 conversion lies in the choice of a porous catalyst with optimized structural features to maximize both the thermodynamics and production capacity.[36, 37]

Single Component Adsorption. Grand canonical Monte-Carlo simulations are utilized to predict the equilibrium gas concentration of carbon dioxide and hydrogen at typical catalytic operating conditions of 300 K and 500 K up to 100 bar. The zeolite structures are assumed rigid with the interactions between the gas and the structure described by the Lennard-Jones potential with additional partial charges. The force field parameters for CO_2 and H_2 within zeolites are well described and have delivered close correlations with experimental data demonstrated by Garcia-Perez *et al.*[38], Babarao *et al.*[39], Lin *et al.*[16], Deeg *et al.*[40] and many others. A summary of the force field parameter values is given in Tables S1 and S2 in Supporting Information. The simulations were performed using the RASPA package.[41]

Mixed Component Adsorption. Competitive adsorption is difficult to simulate because of the complex gas-gas interactions and lack of experimental data. By considering solution thermodynamics the Ideal Adsorbed Solution Theory (IAST) was developed by Myers and Prausnitz to predict the adsorption equilibria of binary mixtures.[42, 43] Perez-Carbajo *et al.*[44] recently demonstrated that IAST could reasonably describe the mixed adsorption of a five-component mixture (CO_2, CH_4, CO, N_2 and H_2) within a range of zeolites (FAU, MFI, MOR and DDR) up to 100 bar. In this study we also consider light gas adsorption within zeolites with minimal surface heterogeneity where IAST is applicable. For more complex adsorbents (especially liquids) and adsorbents where the are adsorbate-specific adsorption sites and non-ideal adsorbate-adsorbate interactions, then the real adsorbed solution theory is necessary, as shown by Erto *et al.*[45]

IAST is typically used to predict the adsorbed ratio of the components given the feed ratio.[46, 47] In our study, we are interested in the inverse problem of predicting the feed ratio necessary to achieve an adsorbed ratio close to the stoichiometry of the reaction of interest. Therefore we have rearranged the model to develop an inverse IAST, see Supporting Information for the mathematical solution.

Table 1 Thermodynamic reaction data for CO_2 conversion scenarios in gas and liquid phase. [1]

Reaction	Gas Phase		Liquid Phase	
	ΔH_{gas} (kJ/mol)	ΔS_{gas} (J/mol)	ΔH_{liquid} (kJ/mol)	ΔS_{liquid} (J/mol)
Formic Acid: $CO_2 + H_2 \rightarrow HCOOH$	15	-87	-31	-195
Formaldehyde: $CO_2 + 2H_2 \rightarrow HCOH + H_2O$	36	-64	-8	-201
Methanol: $CO_2 + 3H_2 \rightarrow H_3COH + H_2O$	-53	-161	-130	-380
Methane: $CO_2 + 4H_2 \rightarrow CH_4 + 2H_2O$	-165	-337	-253	-552

Enthalpy and Entropy of Adsorption. During adsorption the gas transitions from the bulk gas phase to the adsorbed phase with a corresponding change in enthalpy (ΔH) and entropy (ΔS), and consequently the Gibbs free energy ($\Delta G = \Delta H - \Delta S.T$). A larger change in Gibbs free energy is a closer step towards catalytic conversion. Therefore ΔG will be used as a scoring factor along with the amount of adsorbed reactants when selecting the most promising candidates. The change in enthalpy is related to the adsorption energy (U_0) as follows, $\Delta H = U_0 - RT$, where R is the universal gas constant and T is temperature.[48, 49] The change in entropy can be expressed as,

$$\Delta S = \frac{\Delta H}{T} + R \ln \frac{K_H P}{M},$$

where K_H is the Henry's constant, P is pressure and M is the saturation loading. Henry's constant is calculated from the simulation of Widom insertions within the unit cell.[50] While the saturation loading is approximated as the product of the helium pore volume and the liquid density of hydrogen.[48, 51]

The change in enthalpy and entropy upon adsorption is considered a necessary step leading to the full catalytic conversion of carbon dioxide. In this study, we are interested in the catalytic activity of the materials for the reactions listed in Table 1. Thermodynamic data each reaction indicates the changes of enthalpy and entropy when the reaction occurs in the gas and liquid phase.[1] It is important to note that the reactions are all exothermic when carried out in the liquid phase and less input energy is required because of the reduced enthalpy and entropy compared with the gas phase. Considering that the adsorbed phase is a similar state to the liquid phase with an even further reduction in enthalpy and entropy, this is a promising attribute to consider when selecting a zeolite.

Quantitative Structure-Property Relationships

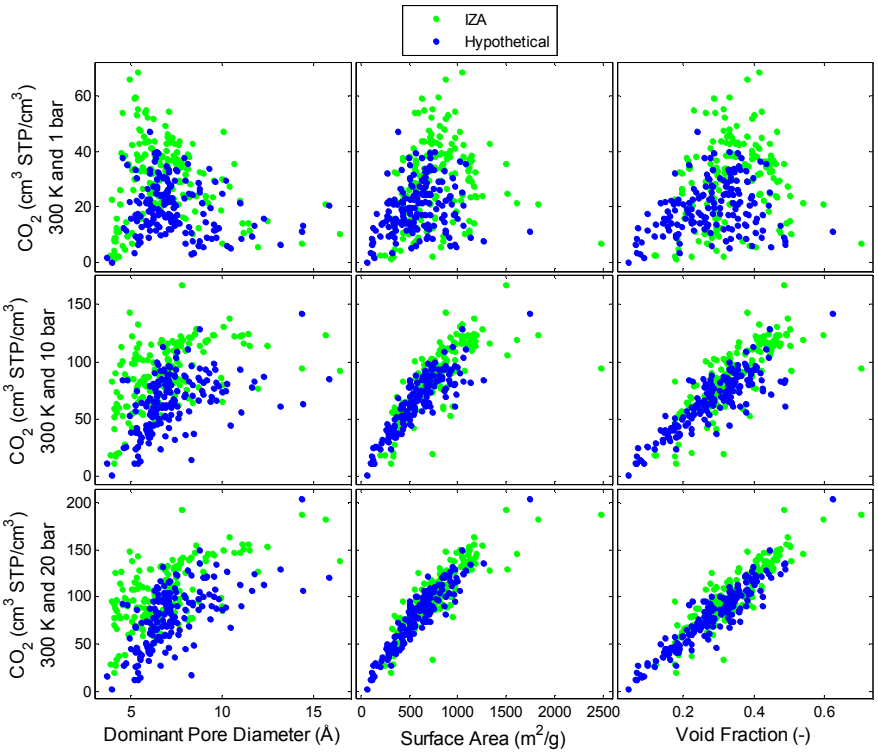

Fig. 2 Simulated CO_2 adsorption uptake in zeolites versus three structural features. Green symbols represent the known zeolites from IZA database and blue symbols represent a diverse subset of the hypothetical zeolite database. Correlation between uptake and void fraction becomes stronger with increasing pressure, and an optimal pore diameter appears at low pressures.

We also employed statistical and machine learning (QSPR) modelling techniques to identify quantitative relationships between the zeolite structural characteristics and the simulated adsorption properties. The modelling methods employ Bayesian methods to optimize the complexity of any nonlinear models, and to therefore optimize the quantitative prediction power of the models. Bayesian methods with sparse priors can also identify the most relevant subsets of structural parameters that have the largest impact on the gas adsorption properties of the zeolites. A complete explanation of these modelling techniques is beyond the scope of this paper, as they have been extensively described in previous publications.[26, 52] In brief, we used a Bayesian regularized feed-forward neural network with three layers, the input nodes, hidden nodes, and output nodes. The input and output nodes employ linear transfer functions, effectively generating a weighted sum of the contributions from the descriptors, or hidden layer nodes respectively. The hidden nodes use a nonlinear sigmoidal transfer function to generate nonlinear models. Bayesian regularization is used to control the degree of nonlinearity of the model to find the best balance between bias (model too simple to capture underlying structure-property relationships) and variance (model overly complex and over fitting). The hidden layer used a small number of nodes (usually 2-3) as the regularization ensures that the number of effective weights (fitted parameters) in the model is relatively independent of the number of hidden layer nodes (and fully connected neural network weights). Models were trained until the Bayesian evidence for the model reached maximum, obviating the need for a validation set to stop neural network training. This machine learning method can model structure-property relationships of arbitrary complexity given sufficient training data. Validation of the predictive power of QSPR models is very important. We held aside 20 % of the data set as an independent test set never used for model development. The models derived from the remaining 80 % of the data were used to predict the performance of zeolites in the test set. In addition, a diverse set of hypothetical structures was used as a training set that was tested on the IZA (International Zeolite Association) set, and vice-versa. The former approach proved more accurate which means that the diverse hypothetical set is a reasonable representation of the complete IZA set. Finally, the combination of the diverse hypothetical set and the IZA set was used as the training set to select a secondary 'smart' set based on an optimal combination of structural features that maximize dual-adsorption properties.

The descriptors for the QSPR model include the maximum pore size, surface area, void fraction, density and heat of adsorption. Heat of adsorption is the isosteric heat of

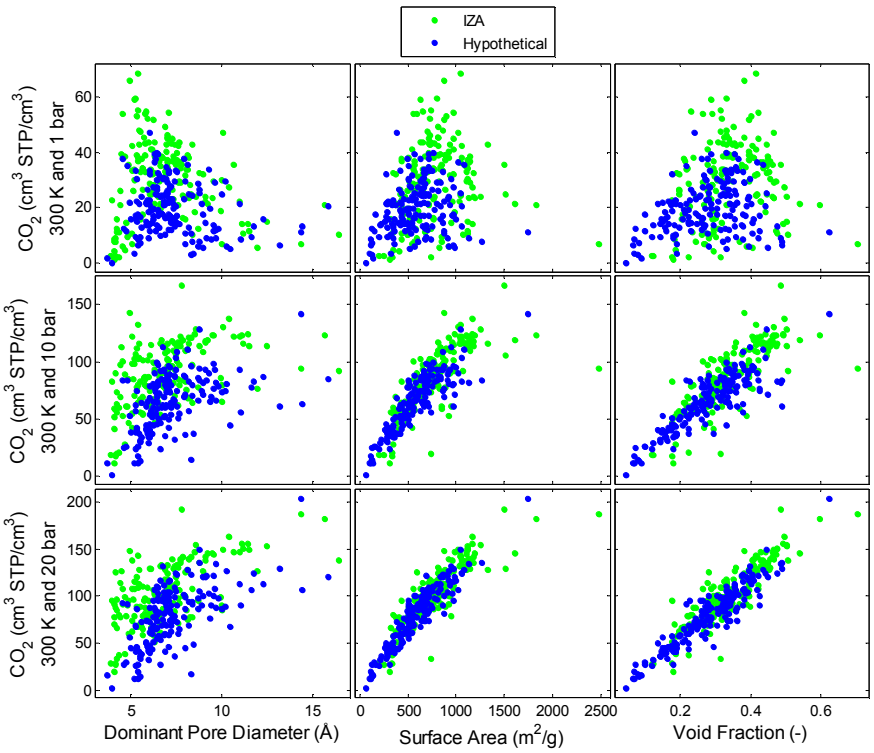

Fig. 3 Simulated H_2 adsorption uptake in zeolites versus three structural features. Green symbols represent the known zeolites from IZA database and blue symbols represent a diverse subset of the hypothetical zeolite database. Correlation between uptake and void fraction becomes stronger with increasing pressure. Correlations do not depend on pressure.

adsorption calculated from the simulation data using $\Delta H = \Delta U - RT$, where ΔU is the energy of adsorption, R is the universal gas constant and T is temperature. Maximum pore size was calculated using the Zeo++ analyzer based on the Voronoi decomposition of the atomic coordinates.[53, 54] Void fraction was calculated using Widom insertions of helium at 300 K based on the Rosenbluth factor described by Smit and Frenkel.[50] While surface area is the accessible surface area based geometrically on a the spherical probe size of nitrogen (3.681 Å), shown to compare well with experimental BET surface areas.[55] In addition to guiding the choice of a 'smart' set, the machine learning method also provides insight into the most important structural parameters.

Results and Discussion

Simulated single component adsorption is viewed as a function of structural descriptors in Figures 2 and 3 for CO_2 and H_2, respectively. The relationships between CO_2 uptake and the structural features depend on pressure. There is a strong linear correlation between CO_2 uptake and void fraction at high pressures (20 bar) while at lower pressures (1 bar) there is a more complex relationship between uptake and pore diameter indicating an optimal pore size that maximizes uptake. The correlations for H_2 on the other hand, do not depend on pressure. There is a strong relationship with void fraction and surface area at all pressures. Similar trends are also observed for volumetric uptake, see Figure S1 and S2 in Supporting Information.

A QSPR model is developed using the following input parameters: temperature, pressure, pore diameter, density, surface area, void fraction and heat of adsorption. The hypothetical dataset is used to train the model which is then tested on the IZA dataset. The model predictions for both CO_2 and H_2 uptake were excellent, with R^2 values of 0.93 and 0.97, respectively shown in Figure 4. The models could predict the gas adsorption with standard errors of 9.5 cm^3 STP/cm^3 (CO_2), and 1.3 cm^3 STP/cm^3 (H_2). We conclude that the hypothetical set with high diversity in pore characteristics is an excellent training set for predicting uptake in all-silica zeolites at a range of temperatures and pressures. When sparse feature selection was imposed, the results indicated that temperature, pressure, density, surface area, and void fraction were the most relevant contributors to the CO_2 and H_2 uptake models. The heat of adsorption was found to be less important for predicting uptake using the QSPR models. However, as will be shown further in the article that heat of adsorption plays a critical role in contributing to the thermodynamics of reaction.

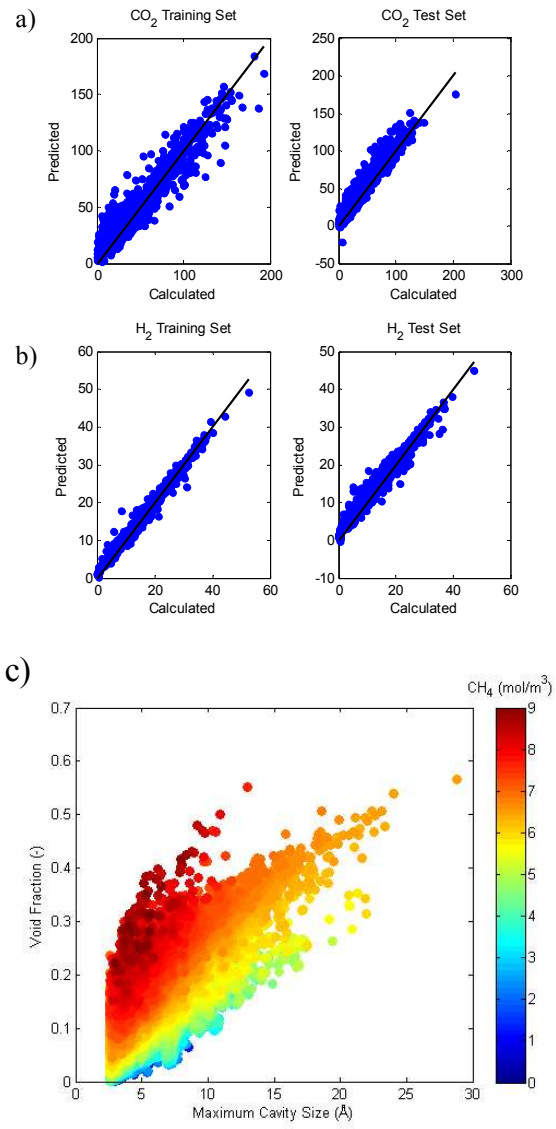

Fig. 4 QSPR nonlinear neural network model predictions for a) CO_2 uptake b) H_2 uptake and c) total dual uptake of CO_2 and H_2 (at 1:4 ratio leading to CH_4 mol produced per m^3 of material) with structural features. Training sets are based on the hypothetical structures and the test sets are based on the IZA structures. The test sets were predicted with high accuracy, R^2 = 0.93 (CO_2), 0.97 (H_2). The total dual uptake is predicted for all 300 thousand based on QSPR extrapolation from structural descriptors.

The simulated pure gas adsorption data is used to predict the dual-adsorption of the mixture through the IAST model. Assuming 100 % yield, the dual-adsorbed mixture converts to a quantity of product. With a 1:1 (CO_2:H_2) stoichiometry, we plot the quantity of formic acid produced at 1 and 10 bar with the corresponding pure gas uptake, see Figure 5. Interestingly, the production of formic acid is hydrogen limited at low pressures and dual-gas limited at higher pressures. This is because at low

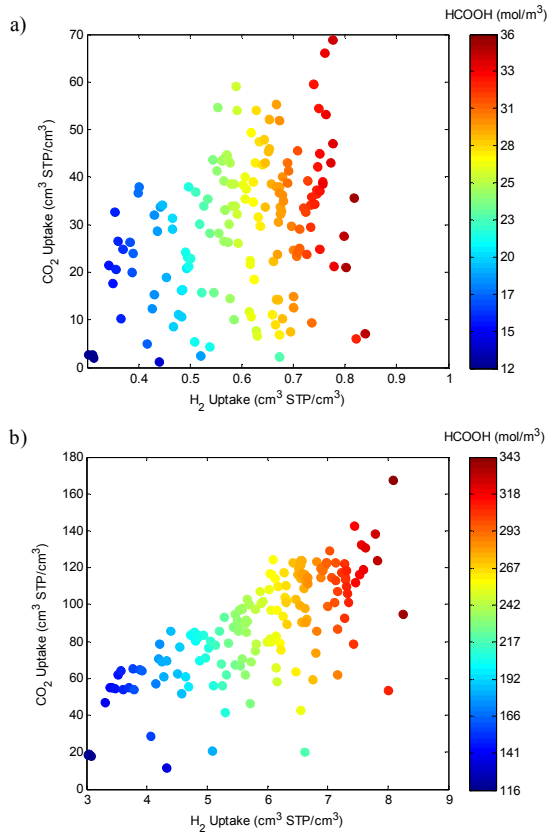

Fig. 5 Stoichiometric dual-adsorption (1:1, CO_2:H_2) as a function of pure CO_2 and H_2 single-adsorption at a) 1 and b) 10 bar, at room temperature for all zeolites. Contour scale is the converted formic acid production (mol/m^3) assuming 100 % yield. Production is hydrogen limited at low pressures and dual-gas limited at higher pressures.

pressures there is a sufficient amount of CO_2 adsorbed while there is insufficient H_2 adsorption. At high pressures on the other hand, there is sufficient uptake of both gases and a more linear dependence is observed.

In a similar manner, the quantity of product is generated for each stoichiometry including formic acid, formaldehyde, methanol and methane that require the stoichiometric adsorption ratios 1:1, 1:2, 1:3 and 1:4 (CO_2:H_2), respectively, see Figure 6a. There is a lot less methane produced than formic acid because methane requires four H_2 molecules per CO_2 rather than a 1:1 ratio. As discussed earlier, hydrogen adsorption is the limiting factor in dual-adsorption for catalysis. As shown from the QSPR model there are many factors that affect the dual-adsorbed quantity including surface area, void fraction and density.

The QSPR neural network model is utilized to select a secondary "smart" set from the 300,000 hypothetical zeolite set with structural features likely to further maximize the adsorption uptake. The neural network-based smart set is shown in Figure 6b, indicating that new structures are discovered with a marginally higher potential for product

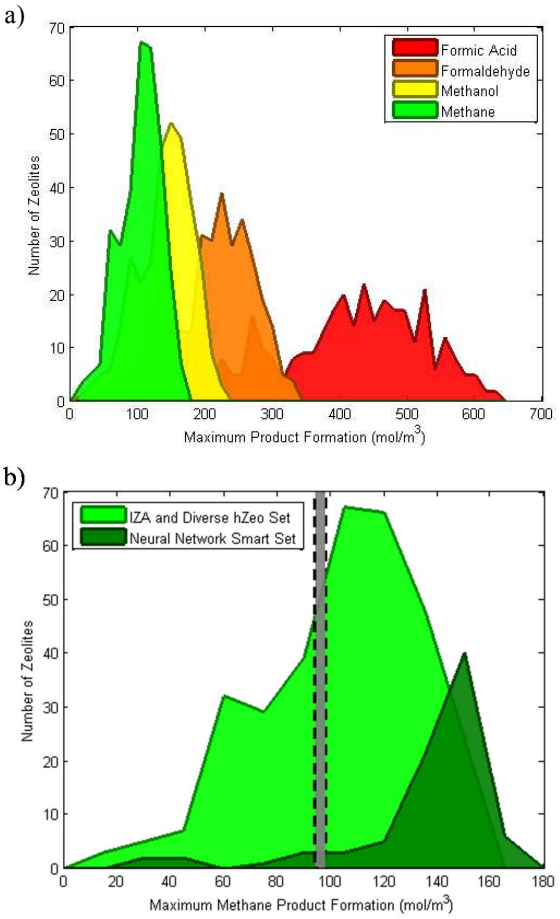

Fig. 6 Distribution of predicted product formation (mol of product/m^3 of zeolite) assuming 100% conversion of all adsorbed reactants. *a*) Formic acid, formaldehyde, methanol and methane that require the stoichiometric adsorption ratios 1:1, 1:2, 1:3 and 1:4 (CO_2:H_2), respectively. *b*) Methane formation with IZA and diverse hypothetical set with neural network-based smart set. Grey section represents conventional product formation from Sabatier Reactors.[2]

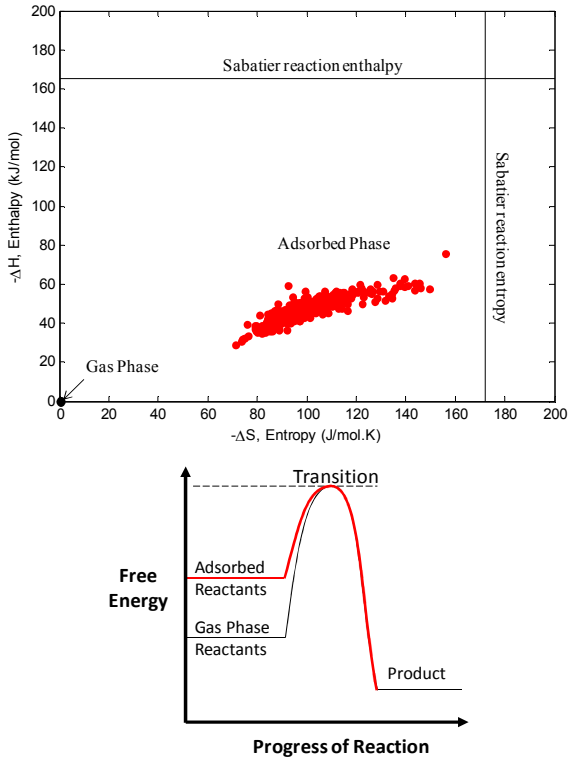

Fig. 7 a) Enthalpy and entropy of reactant adsorption for all zeolites (red dots) compared with experimental enthalpy and entropy of methane production via the Sabatier reaction[2] (black horizontal and vertical lines, respectively). b) Schematic of the reduced energy barrier for reaction as a consequence of adsorption.

formation above the conventional Sabatier reactors that run at a range of operating conditions 10-20 bar and 300-500 K.[2] Note that these estimates are assuming 100 % conversion of all adsorbed gases. In reality this is not the case and the actual conversion efficiency also depends on the energetic landscape, which will be explored using the enthalpy and entropy of adsorption.

The enthalpy and entropy of methane production via the Sabatier reaction (the methanation of CO_2) is measured experimentally to be 165 kJ/mol and 172 J/mol.K, respectively. Here in Figure 7a we plot the predicted change in enthalpy and entropy upon adsorption of the required CO_2 and H_2 ratio. The ulitimate conversion efficienct will depend on the free energy barrier at the transition step which can be different for each zeolite, shown in Figure 7b. However, the adsorbed state does boost the free energy of the system towards the transition state in all cases. Therefore the thermodynamics of physical adsorption is a critical step before the chemical conversion, and materials with a greater change in both entropy and enthalpy of adsorption are more promising candidates for efficient catalysis.

Finally we combine the thermodynamic factors with the degree of production to score the zeolites, see Figure 8. The score factor is the product of the change in Gibbs free energy with quantity of product formation. The top candidates will have a maximum dual-adsorption capacity for the required stoichiometry as well as the large change in enthalpy and entropy in preparation for the catalysis step. When plotted against the structural characteristics void fraction and maximum cavity size, it is evident that there is an optimal range of cavity sizes (~6 Å). It is likely that these cavities offer the correct energetic environment for strong dual-adsorption. Those materials with many of these cavities, characterized by void fraction, will also offer a high production output. Once again, the neural network-based smart set performs higher on the score factor than the randomly chosen set. Theoretically, the neural network model could be retrained with the new data and used to choose a third smart set, a fourth etc. in an

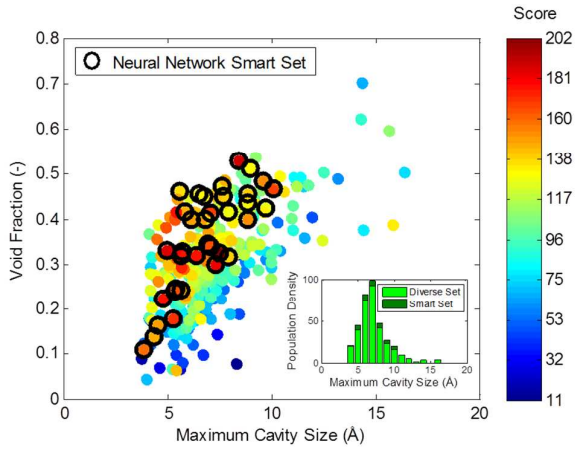

Fig. 8 Catalysis score according to thermodynamics and magnitude of adsorption for methane production (change in Gibbs free energy multiplied by product quantity), plotted with two structural characteristics void fraction and maximum cavity size. Smart set chosen by neural network model is highlighted with black circles. Inset emphasizes the smart set selection of optimal cavity size with population density of cavity sizes for diverse set and smart set.

iterative manner. Here we only demonstrate that one round of neural network selection is sufficient to discover more promising structures.

From this score, five top candidates are chosen and listed in Table 2 for methane production at ambient conditions, while Supporting Information lists candidates for other product formation. The five top candidates provide a diversity in pore shapes and topology. Interestingly there are two ideal silica frameworks, namely PUN and STW, which perform as well as the hypothetical structures. PUN, originally named PKU-9, was first discovered by Peking University with 10-ring and 8-ring channels running in parallel.[56] STW (or SU-32) was synthesized as part of the first family of chiral structures, a useful properties for sorption/separation and catalytic processes.[57] The window size of 3.8 Å is used as a cut-off for methane transport, eliminating structures that would not be capable of exporting the converted product. We observe that the top candidates all have a dominant pore size of ~6 Å with high amounts of void space >30 %.

Thermodynamics play a critical role in determining the optimal catalyst however kinetics is also an important factor that includes reaction, desorption and diffusion rates. We have shown that there is an optimal cavity size to maximize the dual adsorption properties but the optimal pore size for diffusion is yet to be determined. During operation the reactants will adsorb within the catalyst, react into products and exit by diffusion. The molecular diameter of the products considered here are larger than the reactants and therefore the diffusion of the product could be the rate-limiting determinant. The screening procedure presented here has discarded those structures that would not allow the products to diffuse through due to the restrictive window size. Other factors to consider include tortuosity that could increase the resistance of product diffusion unnecessarily, pore shape that could be unfavourable for product orientation and pore uniformity where fluctuations in pore diameter could present multiple energy barriers that could further inhibit product flow. An ideal zeolitic structure for catalyst would consist of a stable and highly connected network of pores with maximum porosity and optimal pore size (or range of sizes) for adsorption, reaction and diffusion. Overall, it is very difficult to consider all factors when determining the optimal catalyst but this preliminary screening procudure is a reasonable step forward.

Future work includes the incorporation of ions to further encourage catalytic activity. The porosity templates investigated here are a good basis for this future work. The interaction between gases and ions have been modelled well by Garcia-Sanchez *et al.*[58], Kim *et al.*[59] and Darkrim *et al.*[60], establishing the ground-work for the next stage of screening. The addition of by-product water must also be considered which could hinder the transport of products, adsorption of pre-cursors and reaction kinetics. In addition, quantum-based calculations could accurately predict the activation energy for catalysis, adding an additional layer to the screening procedure. This concept has been discussed in other virtual screening studies to optimize the computational time for large amounts of materials by hierarchically laying the different computational routines with varying accuracy and computational time.[12, 61] In these procedures, less accurate but fast calculations are performed first to narrow the scope of structures, followed by more accurate but slower calculations to further narrow the amount of promising candidates to a synthesizable number. Ultimately, neural network-based decision-making can play a role in scaling this screening process to an indefinite amount of materials where structural descriptors are calculated almost instantaneously. Given the continually growing databases of new materials through programs such as the Materials Genome Initiative, a scalable screening strategy is necessary to manage large amounts of data. In this work, the first procedure steps are mapped and demonstrated for choosing promising catalysis templates for carbon dioxide utilization.

Conclusions

A virtual screening procedure is mapped and utilized to discover the optimal zeolite templates for conversion of carbon dioxide into useful products. Over 300 thousand structures with varying porosity features are screened using a combination of GCMC adsorption simulations, IAST dual-adsorption models, energy-entropy calculations and neural network-based QSPR models. Top candidates are listed for the production of methane, methanol, formic acid and formaldehyde, all requiring different stoichiometric adsorption ratios of carbon dioxide and hydrogen.

Robust structure-property relationships are found between structural descriptors such as pore size, surface area and void fraction, and zeolite performance. Neural network-based QSPR models were valuable in identifying more promising

Table 1 Top candidates with the overall performance in formation quantity and favourable energetics for methane production at ambient conditions.

Details	Side View	Front View
h8315435 Density (g/cm^3) = 1.44 Restricting Window Size (Å) = 3.90 Max Cavity Size (Å) = 7.50 Void Fraction (-) = 0.33 Surface Area (m^2/g) = 924 CO_2 Heat of Adsorption (kJ/mol) = 38.7 H_2 Heat of Adsorption (kJ/mol) = 6.79	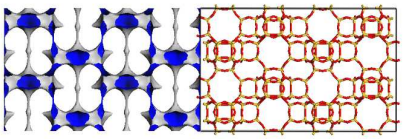	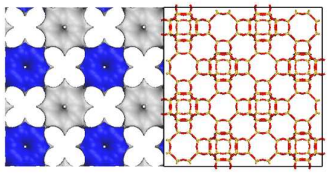
h8287217 Density (g/cm3) = 1.38 Restricting Window Size (Å) = 7.78 Max Cavity Size (Å) = 8.44 Void Fraction (-) = 0.53 Surface Area (m2/g) = 882 CO_2 Heat of Adsorption (kJ/mol) = 23.0 H_2 Heat of Adsorption (kJ/mol) = 5.5	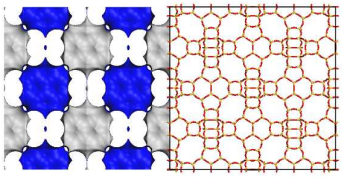	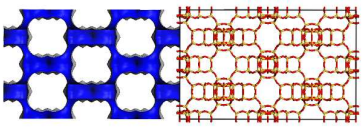
PUN Density (g/cm3) = 1.49 Restricting Window Size (Å) = 3.95 Max Cavity Size (Å) = 4.98 Void Fraction (-) = 0.44 Surface Area (m2/g) = 780 CO_2 Heat of Adsorption (kJ/mol) = 22.9 H_2 Heat of Adsorption (kJ/mol) = 6.2	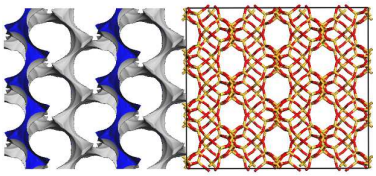	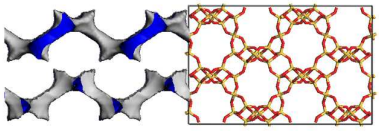
STW Density (g/cm3) = 1.64 Restricting Window Size (Å) = 4.82 Max Cavity Size (Å) = 5.37 Void Fraction (-) = 0.42 Surface Area (m2/g) = 1040 CO_2 Heat of Adsorption (kJ/mol) = 14.1 H_2 Heat of Adsorption (kJ/mol) = 1.57	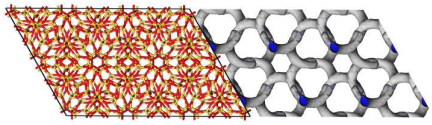	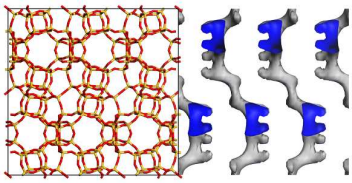
h8123219 Density (g/cm3) = 1.41 Restricting Window Size (Å) = 4.42 Max Cavity Size (Å) = 6.91 Void Fraction (-) = 0.34 Surface Area (m2/g) = 1022 CO_2 Heat of Adsorption (kJ/mol) = 19.0 H_2 Heat of Adsorption (kJ/mol) = 5.5	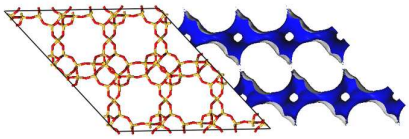	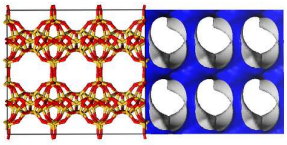

candidates from a growing set of zeolite frameworks. Top candidates have a common cavity size of around 6 Å, which maximizes the strength of dual-adsorption with a maximum void space greater than 30 % to increase product quantity.

Future work includes the incorporation of water (by-product), ions to enhance catalytic activity and quantum mechanics-based calculations to accurately determine reaction kinetics and finally synthetic trial.

Acknowledgements

AWT, DAW, MSL and DFK acknowledge the support of the CSIRO Advanced Materials, Computational & Simulation Sciences, and Intelligent Processing Transformational Capability Platforms. AWT and DFK acknowledge the Science and Industry Endowment Fund for support through the 'Solving the Energy-Waste Roadblock' project. MH was supported by the U.S. Department of Energy, Office of Basic Energy Sciences, Division of Chemical Sciences, Geosciences and Biosciences under Award DE-FG02-12ER16362.

Notes and references

1. P. Styring, E. A. Quadrelli and K. Armstrong, *Carbon Dioxide Utilisation: Closing the Carbon Cycle*, Elsevier, 2015.
2. W. Wang, S. Wang, X. Ma and J. Gong, *Chem. Soc. Rev.*, 2011, **40**, 3703-3727.
3. M. Z. Jacobson, *Energ. Environ. Sci.*, 2009, **2**, 148-173.
4. N. von der Assen, J. Jung and A. Bardow, *Energ. Environ. Sci.*, 2013, **6**, 2721-2734.
5. E. J. Maginn, *J. Phys. Chem. Lett.*, 2010, **1**, 3478-3479.
6. Y. Xie, T.-T. Wang, X.-H. Liu, K. Zou and W.-Q. Deng, *Nat. Commun.*, 2013, **4**, 1960.
7. P. Lanzafame, G. Centi and S. Perathoner, *Chem. Soc. Rev.*, 2014, **43**, 7562-7580.
8. X. Meng, T. Wang, L. Liu, S. Ouyang, P. Li, H. Hu, T. Kako, H. Iwai, A. Tanaka and J. Ye, *Angew. Chem.*, 2014, **126**, 11662-11666.
9. S. Moret, P. J. Dyson and G. Laurenczy, *Nat. Commun.*, 2014, **5**.
10. X. Meng, T. Wang, L. Liu, S. Ouyang, P. Li, H. Hu, T. Kako, H. Iwai, A. Tanaka and J. Ye, *Angew. Chem.*, 2014, DOI: 10.1002/ange.201404953.
11. J. Graciani, K. Mudiyanselage, F. Xu, A. E. Baber, J. Evans, S. D. Senanayake, D. J. Stacchiola, P. Liu, J. Hrbek, J. F. Sanz and J. A. Rodriguez, *Science*, 2014, **345**, 546-550.
12. Y. J. Colon and R. Q. Snurr, *Chem. Soc. Rev.*, 2014, **43**, 5735-5749.
13. R. H. Crabtree, *Chem. Commun.*, 1999, DOI: 10.1039/A901022J, 1611-1616.
14. D. Dubbeldam, R. Krishna, S. Calero and A. Ö. Yazaydın, *Angew. Chem. Int. Ed.*, 2012, **51**, 11867-11871.
15. A. W. Thornton, D. Dubbeldam, M. S. Liu, B. P. Ladewig, A. J. Hill and M. R. Hill, *Energ. Environ. Sci.*, 2012, **5**, 7637-7646.
16. L.-C. Lin, A. H. Berger, R. L. Martin, J. Kim, J. A. Swisher, K. Jariwala, C. H. Rycroft, A. S. Bhown, M. W. Deem, M. Haranczyk and B. Smit, *Nat. Mater.*, 2012, **11**, 633-641.
17. C. E. Wilmer, O. K. Farha, Y.-S. Bae, J. T. Hupp and R. Q. Snurr, *Energ. Environ. Sci.*, 2012, **5**, 9849-9856.
18. P. Canepa, C. A. Arter, E. M. Conwill, D. H. Johnson, B. A. Shoemaker, K. Z. Soliman and T. Thonhauser, *J. Mater. Chem. A*, 2013, **1**, 13597-13604.
19. Y. Zhang, S. Yang, Y. Jiao, H. Liu, H. Yuan, S. Lu, T. Ran, S. Yao, Z. Ke, J. Xu, X. Xiong, Y. Chen and T. Lu, *J. Chem. Inf. Model,*, 2013, **53**, 3163-3177.
20. C. E. Wilmer, M. Leaf, C. Y. Lee, O. K. Farha, B. G. Hauser, J. T. Hupp and R. Q. Snurr, *Nat Chem*, 2011, **4**, 83-89.
21. C. Baerlocher and L. B. McCusker, Database of Zeolite Structures, www.iza-structure.org/databases/).
22. M. W. Deem, R. Pophale, P. A. Cheeseman and D. J. Earl, *J. Phys. Chem. C*, 2009, **113**, 21353-21360.
23. L. J. Abbott, N. B. McKeown and C. M. Colina, *J. Mater. Chem. A*, 2013, **1**, 11950-11960.
24. Z. Xiang and D. Cao, *J. Mater. Chem. A*, 2013, **1**, 2691-2718.
25. M. Calvaresi and F. Zerbetto, *J. Mater. Chem. A*, 2014, **2**, 12123-12135.
26. T. Le, V. C. Epa, F. R. Burden and D. A. Winkler, *Chem. Rev.*, 2012, **112**, 2889-2919.
27. M. Fernandez, T. K. Woo, C. E. Wilmer and R. Q. Snurr, *J. Phys. Chem. C*, 2013, **117**, 7681-7689.
28. V. C. Epa, A. L. Hook, C. Chang, J. Yang, R. Langer, D. G. Anderson, P. Williams, M. C. Davies, M. R. Alexander and D. A. Winkler, *Adv. Funct. Mater.*, 2014, **24**, 2085-2093.
29. M. Salahinejad, T. C. Le and D. A. Winkler, *J. Chem. Inf. Model,*, 2013, **53**, 223-229.
30. M. Salahinejad, T. C. Le and D. A. Winkler, *Mol. Pharm.*, 2013, **10**, 2757-2766.
31. V. C. Epa, J. Yang, Y. Mei, A. L. Hook, R. Langer, D. G. Anderson, M. C. Davies, M. R. Alexander and D. A. Winkler, *J. Mater. Chem.*, 2012, **22**, 20902-20906.
32. V. C. Epa, F. R. Burden, C. Tassa, R. Weissleder, S. Shaw and D. A. Winkler, *Nano Lett.*, 2012, **12**, 5808-5812.
33. C. Baerlocher and L. B. McCusker, *Journal*, 2011.
34. R. Pophale, P. A. Cheeseman and M. W. Deem, *Phys. Chem. Chem. Phys.*, 2011, **13**, 12407-12412.
35. R. L. Martin, B. Smit and M. Haranczyk, *J. Chem. Inf. Model,*, 2011, **52**, 308-318.
36. D. J. Parrillo and R. J. Gorte, *Catal. Lett.*, 1992, **16**, 17-25.
37. N. Sun, X. Wen, F. Wang, W. Wei and Y. Sun, *Energ. Environ. Sci.*, 2010, **3**, 366-369.
38. E. García-Pérez, J. B. Parra, C. O. Ania, A. García-Sánchez, J. M. Baten, R. Krishna, D. Dubbeldam and S. Calero, *Adsorption*, 2007, **13**, 469-476.
39. R. Babarao, Z. Hu, J. Jiang, S. Chempath and S. I. Sandler, *Langmuir*, 2007, **23**, 659-666.
40. K. S. Deeg, J. J. Gutiérrez-Sevillano, R. Bueno-Pérez, J. B. Parra, C. O. Ania, M. Doblaré and S. Calero, *J. Phys. Chem. C*, 2013, **117**, 14374-14380.
41. D. Dubbeldam, S. Calero, D. E. Ellis and R. Q. Snurr, *Mol. Simulat.*, 2015, **0**, 1-21.
42. J. A. O'Brien and A. L. Myers, *Ind. Eng. Chem. Res.*, 1988, **27**, 2085-2092.
43. A. L. Myers and J. M. Prausnitz, *AIChE J.*, 1965, **11**, 121.
44. J. Perez-Carbajo, P. Gomez-Alvarez, R. Bueno-Perez, P. J. Merkling and S. Calero, *Phys. Chem. Chem. Phys.*, 2014, **16**, 5678-5688.
45. A. Erto, A. Lancia and D. Musmarra, *Micropor. Mesopor. Mat.*, 2012, **154**, 45-50.
46. J. Chen, L. S. Loo and K. Wang, *J. Chem. Eng. Data*, 2011, **56**, 1209-1212.
47. J. A. Swisher, L.-C. Lin, J. Kim and B. Smit, *Aiche Journal*, 2013, **59**, 3054-3064.
48. C. M. Simon, J. Kim, L.-C. Lin, R. L. Martin, M. Haranczyk and B. Smit, *Phys. Chem. Chem. Phys.*, 2014, **16**, 5499-5513.
49. S. Sircar, R. Mohr, C. Ristic and M. B. Rao, *J. Phys. Chem. B*, 1999, **103**, 6539-6546.
50. D. Frenkel and B. Smit, *Understanding molecular simulation: From algorithms to applications*, Academic Press, San Diego, 2002.
51. A. L. Myers, *Colloid Surface A*, 2004, **241**, 9-14.
52. F. R. Burden and D. A. Winkler, *QSAR & Combinatorial Science*, 2009, **28**, 1092-1097.
53. M. Haranczyk, C. H. Rycroft, R. L. Martin and T. F. Willems, *Journal*, 2012.
54. T. F. Willems, C. H. Rycroft, M. Kazi, J. C. Meza and M. Haranczyk, *Micropor. Mesopor. Mat.*, 2012, **149**, 134-141.
55. T. Duren, F. Millange, G. Ferey, K. S. Walton and R. Q. Snurr, *J. Phys. Chem. C*, 2007, **111**, 15350-15356.
56. J. Su, Y. Wang, Z. Wang and J. Lin, *J. Am. Chem. Soc.*, 2009, **131**, 6080-6081.

57. L. Tang, L. Shi, C. Bonneau, J. Sun, H. Yue, A. Ojuva, B.-L. Lee, M. Kritikos, R. G. Bell, Z. Bacsik, J. Mink and X. Zou, *Nat. Mater.*, 2008, **7**, 381-385.
58. A. García-Sánchez, C. O. Ania, J. B. Parra, D. Dubbeldam, T. J. H. Vlugt, R. Krishna and S. a. Calero, *J. Phys. Chem. C*, 2009, **113**, 8814-8820.
59. J. Kim, L.-C. Lin, J. A. Swisher, M. Haranczyk and B. Smit, *J. Am. Chem. Soc.*, 2012, **134**, 18940-18943.
60. F. Darkrim, A. Aoufi, P. Malbrunot and D. Levesque, *J. Chem. Phys.*, 2000, **112**, 5991-5999.
61. T. Watanabe and D. S. Sholl, *Langmuir*, 2012, **28**, 14114-14128.